University of Brasília – UnB

Faculty of Science and Technology in Engineering

Postgraduate Program in Integrity of Materials Engineering

Computational simulation of a plasma thruster for picosatellites

Renan Almeida de Souza

Advisor: Prof. Dr. Rodrigo Andrés Miranda Cerda

University of Brasília – UnB
Faculty of Science and Technology in Engineering

Computational simulation of a plasma thruster for picosatellites

Renan Almeida de Souza

Advisor: Prof. Dr. Rodrigo Andrés Miranda Cerda

Master Thesis in Integrity of Materials Engineering Issue: 115A/2025

Brasília/DF, February 2025

University of Brasília – UnB
Faculty of Science and Technology in Engineering
Postgraduate Program in Integrity of Materials Engineering

Computational simulation of a plasma thruster for picosatellites

Renan Almeida de Souza

Master's thesis submitted to the postgraduate program in Integrity of Materials Engineering at University of Brasilia, as part of the requirements for obtaining a master's degree.

Approved by:

Prof. Dr. Rodrigo Andrés Miranda Cerda
Advisor

Prof. Dr. Eliel Eleuterio Farias
Examiner - UFRR

Profa. Dra. Gabriela Cunha Possa
Examiner - FCTE/UnB

Report (minutes) of the dissertation defense electronically signed by the examination committee, via the Electronic Information System (SEI), document 12384165, process 23106.012024/2025-95.

Brasília/DF, February 2025

Catalographic Card

Souza, R. A.
Computational simulation of a plasma thruster for picosatellites
[Distrito Federal], 2025.
39p., 210 × 297 mm (FCTE/UnB Gama, Master in Integrity of Materials Engineering, 2025).
Master Thesis - University de Brasília.
Faculdade do Gama

1. Electric Propulsion
2. Plasmas
3. Picosatellite
4. Ions

I. ENC/FCTE/UnB.
II. Title (series)

Reference

Souza, R. A. (2025). Computational simulation of a plasma thruster for picosatellites. Master's Thesis in Integrity of Engineering Materials, Publication 115A/2025, Postgraduate Program, Faculty of Science and Technology in Engineering, University of Brasília, Brasília, DF, 39p.

souzaalmeidarenan@gmail.com

Brasília, DF – Brazil

Acknowledgements

After my undergraduate and postgraduate studies, cultivating interpersonal relationships has proven to be the ideal tool for achieving my dreams. I would like to express my gratitude to everyone who has supported me in this new stage.

My family is my safe haven and I am absolutely certain that I can count on you. I would like to especially thank Edilene Almeida Braz, my mother, and Mateus Bezerra de Souza, my father, and Raphael Almeida de Souza, my brother, for showing me how to pursue my dreams and how to be a better person. The support and encouragement I have received and continue to receive from you only shows how capable I am of achieving all of my life's projects. I would like to thank my teachers, who gave me the necessary encouragement to make me feel ready to take on new challenges. The academic support I received from everyone resulted in my motivation in the academic environment. I would especially like to thank Rodrigo Andres Miranda Cerda for allowing me to be independent in the production of this work. His guidance showed me a new world in the area of scientific research.

Last but not least, I would especially like to thank all my friends. Just like the seasons, your different personalities have shown me the plurality of the world, as well as the different solutions that a problem can have. I thank each of you who listen to me and give me advice on how to follow my path. I thank you for encouraging me and recognizing my hard-earned achievements. The support I receive from you has made me understand the difference between relatives and family members and how much I should value each one of you.

I would like to especially thank Camila Boniolo, Amanda Oliveira and the Illuminati (Iago, Matheus, Tamara, Keterly, Stefany, Keterly, Luisa, Larissa and Gabriel). I am certain that no matter where we are, we will always be a family. I would like to thank my beloved Mylena Rodrigues and Mariana Martins for having accompanied me and encouraged me in all my life projects and especially for not giving up on me and for making me realize that we do have a world to conquer. I would like to thank Luiz George, Claudio Corrêa and Guilherme Richard for always worrying about my achievements and being pillars of this path. I would like to thank Mel Schiavi, Isaque Pires and Nina Alt for having taught me to run and not give up on my dreams since high school.

To the friends I was able to meet thanks to Zenit Aerospace: my lovely godmother Eduarda Tavares, Lucas Rodrigues, Debora Cairo, Adriano Fonseca, Thiago Vinicius, Pedro Lucas, Maria Claudia, Julia Ribeiro, Thamiris Libard, Lucas Moacir, Marco Lins, Arthur Loureiro among everyone in this huge family. To all the friends I was able to meet through the PASCH project, where they also encouraged me and helped me in every way to achieve my goals. Thank you Lúcia Alt, my beloved mentor, Julia Moreschi, Amanda Marasca, Maria Clara, Leonardo Rocha, Laura Martins, Leticia Schröter, Josh Coe, Maria Clara, Maria Fernanda and everyone who walked the trail with me.

Thank you Camila Gomes for introducing me to the world of dance and also being an independent partner in projects, your tips and insights have always helped me focus on my goals. Thank you also Pedro Lobato, Gabriel Santana, Marcos Moura, Maria Clara, Ana Paula, Nicole Marioto, Luiza Guido, Pedro Guido, Doug, you brought me a new vision of how I could deal with my problems and also thank you for all the emotional support.

Thank you for showing me that every human being has their own struggles. Thank you for showing me that you are trying to overcome your difficulties, no matter how long it takes. I am following each one of you and I am also with you on this path. This helps me more and more to continue on my path. I thank you for being who you are and for being with me, supporting me in the worst and best moments, you inspire.

Simulação computacional de um propulsor a plasma para satélites miniaturizados

Resumo

Propulsores elétricos, também conhecidos como propulsores a plasma, representam um tipo de dispositivo de propulsão espacial que utiliza forças eletromagnéticas para gerar empuxo. Os propulsores a plasma apresentam diversas vantagens em relação à propulsão química, como alto impulso específico e alta eficiência, sendo comumente empregados para manutenção de posição de satélites, manobras de transferência orbital e missões no espaço profundo.

A popularização de mini e microssatélites em missões espaciais de baixo custo resultou em um interesse crescente no desenvolvimento de propulsores de baixa potência. O propulsor ambipolar é um tipo de propulsor a plasma que é simples de construir e pode ser escalado para dimensões menores e potências operacionais reduzidas. Nesta tese, é proposta uma versão reduzida do propulsor ambipolar para satélites miniaturizados, comercialmente conhecidos como "PocketQube". Simulações numéricas são realizadas para obter o impulso específico, que é um parâmetro importante para a avaliação de propulsores. São discutidas potenciais aplicações dessa tecnologia, como extensão de missões espaciais e desorbitamento. Os resultados apresentados podem representar uma contribuição para o desenvolvimento de tecnologias espaciais.

Palavras-chave: Propulsão elétrica, plasma, picosatellite.

Abstract

Electric thrusters, also known as plasma thrusters, represent a type of space propulsion devices that employ electromagnetic forces to generate thrust. Plasma thrusters have a number of advantages compared to chemical propulsion, for example, high specific impulse and high efficiency, and are commonly employed for station-keeping of satellites, orbit transfer maneuvers and deep-space missions.

The popularization of mini and microsatellites in low-cost space missions have resulted in a growing interest in the development of low-power thrusters. The ambipolar thruster is a type of plasma thruster which is simple to construct and can be scaled to smaller dimensions and lower operational powers. In this thesis a reduced version of the ambipolar thruster is proposed for miniaturized satellites, commercially known as "PocketQube". Numerical simulations are performed to obtain the specific impulse, which is an important parameter for the evaluation of thrusters. Potential applications of this technology are discussed, for example, extending space missions, and de-orbiting. The results presented here can represent a contribution to the development of space technologies.

Keywords: Electric Propulsion, plasma, picosatellite

Contents

List of Tables

List of Figures

List of Nomenclatures and Abbreviations

APT Ambipolar Plasma Thruster

CPS Chemical Propulsion System

CS CubeSat

EPS Electric Propulsion System

ECRT Electron Cyclotron Resonance Thruster

FEMM Finite Element Method Magnetics

GEO Geostationary Orbit

GTO Geostationary Transfer Orbirt

GIT Gridded Ion Thrusters

HDLT Helicon Double Layer Thruster

HPT Helicon Plasma Thruster

HET Hall Effect Thruster

LPF-UnB Laboratory of Plasma Physics at Unb

LTE Local Thermodynamic Equilibrium

LEO Low Earth Orbit

MSU Morehead State University

PIC Particle-in-Cell

PQ PocketQube

RF Radiofrequency

STK System Tool Kit

XOOPIC X-Windows Object-Oriented Particle-in-Cell code

1 Introduction

The miniaturization of satellite technology has led to the development of smaller systems such as CubeSat (CS) and, more recently, PocketQube (PQ) (Bouwmeester et al., 2020). Over the past years, miniature satellite systems have experienced a surge being adopted across governmental, academic, and commercial sectors. What originated as experimental platforms for testing emerging space technologies and training aerospace engineering students has matured into an industrial ecosystem (Zanola, 2019). Commercial enterprises now operate fleets of these compact orbital devices as core components of profitable Earth monitoring services, with particular growth in multispectral imaging applications for agriculture, urban planning, and environmental tracking (Mueller et al., 2010)(Tummala and Dutta, 2017).

Miniaturization in space field was possible due to a standarized process of miniaturization that was a requirement for the so called, CS, with 100x100x100 mm size and it is also adaptable for a multiple combination to enhance technology usage (Alfriend et al., 2009). This competitive market gave birth to a new development for spacecraft subsystems and propulsion or micro propulsion became an essential asset for spacecraft lifespan (Leomanni et al., 2017).

According to Laufer and Pelton (2019), the term "pico satellite" refers to satellites with range in mass from 100g to 1kg. In 2009, professor, Robert J. Twiggs in a project with Morehead State University (MSU) and Kentucky Space designed the first PQ which is a system with a maximum weight of 250g and 50x50x50 mm, these are considered to fit in the pico spectrum of spacecraft (Bouwmeester et al., 2017).

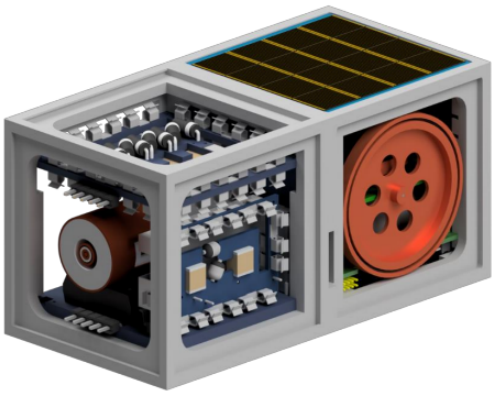

Figure 1.1. 2P PQ example. Source: Sammut et al. (2019)

The constrains available for PQ were defined in 2018 and focused on mechanical dimensions and interfaces (Bouwmeester et al., 2020). This system is designed to host payloads with a depth

constrain requirement, for instance optical instruments and electric propulsion.

The usage of PQ is limited due to its dimensions. According to Mejía-Kaiser (2020) in Space Debris Mitigation, there are some maneuver mechanisms, such as de-orbiting with electric propulsion systems, that are able to limit the presence of PQ in orbits, but with high risks in long missions.

Therefore, it is recommended to launch PQ into low orbits, where the electric propulsion system will maintain its orbit and de-orbiting occur naturally (Sammut et al., 2019). However, due to current technology status, the Electric Propulsion System (EPS) is developed as the payload of the spacecraft. This challenges dealing with small sizes will propose a new creative thinking to overcome new applications and components miniaturization, such as propulsion systems. Before diving into the Ambipolar Plasma Thruster (APT), the next chapter will state some plasma parameters to further analysis in the simulation.

While these spacecrafts have demonstrated significant potential in space applications, their operational capabilities remain limited due to constraints in propulsion systems. Propulsion systems must be able to downscale to offer same efficiency (Sammut et al., 2019). EPS has emerged as a promising solution for small satellite maneuvering, offering high specific impulse and extended operational lifetimes compared to chemical propulsion. However, the challenge lies in adapting EPS for platforms as small as PQ without compromising performance (Silva et al., 2018). It has a performance known by low thrust, high specific impulse, and limited moving parts.

APTs have gained attention as viable propulsion solutions due to their simplicity, lack of electrodes, and potentially long operational lifetime (Miranda et al., 2019)(Sheehan et al., 2015). Compared to other EPS technologies such as Hall Effect Thruster (HET) and Gridded Ion Thrusters (GIT), APTs offer reduced system complexity and cost. While CS -scale APT have been investigated in prior research, the feasibility of further miniaturizing such a system to the PQ scale remains largely unexplored. Initial investigation on Helicon Plasma Thruster (HPT) began with Boswell at Australian National University in 2000s (Levchenko et al., 2020)(Jahn, 2006).

This thesis aims to propose an initial assessment of the feasibility of miniaturizing an APT for a PQ through numerical simulations and system-level mission analysis. The study will employ a Particle-in-Cell (PIC) code for plasma behavior analysis, Finite Element Method Magnetics (FEMM) for magnetic field distribution modeling, and System Tool Kit (STK) for preliminary orbital prediction. The focus will be on characterizing plasma density influences, magnetic field alterations, ion and electron velocities, and electric potential within the thruster.

Unlike previous studies, which analyze the full performance of APTs on larger satellite platforms, this research will focus on plasma production within a miniaturized system and the associated constraints (van Lynden, 2023). A brief comparison with CS, APTs will be included for context in the introductory chapters but will not form a major component of the study. Additionally, no power-level variations in plasma production will be analyzed at this stage.

A conceptual mission analysis will be proposed to explore potential PQ applications for a

miniaturized APT. This will be based on existing mission examples in the literature adapted for the constraints identified in the simulations. The results of this study are expected to provide insight into the fundamental scaling challenges of APT miniaturization and define constraints that could guide future experimental validation efforts.

1.1 Research proposal

1.1.1 Main Objective

This work has as main objective to perform a theoretical study of an APT for a PQ.

Therefore it is proposed how to best adapt the current HPT experiment at the Laboratory of Plasma Physics at Unb (LPF-UnB) for a PQ propulsion subsystem through numerical simulation.

1.1.2 Specific Objectives

Following the main objectives, the specific objectives are defined:

- Construct a two-dimensional model of the plasma in an APT with reduced dimensions compatible with a PQ.
- Perform numerical simulations of this model using the PIC method.
- Obtain plasma diagnostics from the numerical simulations for validation with future experimental tests
- Obtain performance parameters for comparison and evaluation.

This work is structured as follows: first, the brief review of Picosatellites in chapter 2, how they have changed the space subsystems development. The definition of plasma and its parameters are explained in chapter 3. Chapter 4 is a deep understanding of engineering impacts on thrusters development. A deep description of APT is defined in chapter 5. The computational simulation is defined and all steps are explained in chapter 6. At least chapter 7 and 8 state the results and propose a discussion with possible future research on the area.

2 Plasma Physics Theory

To achieve a comprehensive understanding of plasma thruster operation, it is essential to first grasp the fundamental concepts of plasma physics. This chapter presents the core principles and methodologies that form the basis for explaining the phenomena discussed throughout this thesis.

2.1 Definition and properties

Almost all ordinary matter in the universe consists of plasma (Bittencourt, 2013). According to Chen et al. (1984), plasma is defined as a quasi-neutral gas composed of charged particles and neutrals that exhibit collective behavior. The charged particles in a plasma typically include ions and electrons. To be classified as plasma, three criteria must be considered: the net charge of the plasma, the plasma parameter, and the plasma frequency, as described below.

2.1.1 Neutrality and Debye Shielding

Whenever a charge is introduced into a plasma, the oppositely charged particles rearrange themselves into a cloud to neutralize the electrostatic field. This shielding cloud effectively diminishes the influence of the electric field and forms over a distance approximately equal to the Debye length, λ_D.

$$\lambda_D = \left(\frac{\epsilon_0 K T_e}{n e^2} \right)^{1/2} \tag{2.1}$$

where ϵ represents the permittivity of free space, K denotes Boltzmann's constant, T_e is the electron temperature, n is the plasma density, and e corresponds to the fundamental charge. When the characteristic dimension of the system L satisfies $L \gg \lambda_D$, any disturbances of the local charge concentration or externally introduced potentials are protected within a distance much smaller than L. This isolation preserves the quasineutrality of the plasma by limiting the penetration of the external electric field, as expressed by Equation 2.2.

$$\lambda_D << L \tag{2.2}$$

2.1.2 Collective behavior

The first criterion is valid only if there is a sufficient number of particles within the Debye sphere; otherwise, it cannot be considered a statistically valid concept. This phenomenon is commonly referred to as collective particle shielding or collective behavior.

$$N_D = \frac{4}{3} n \pi \lambda_D^3 = 1.38 \times 10^6 \frac{T^{\frac{3}{2}}}{\sqrt{n}} \tag{2.3}$$

The number of particles within a Debye sphere N_D is quantified by Equation 2.3, with the criterion requiring that this value significantly exceeds unity ($N_D \gg 1$).

2.1.3 Plasma Frequency

The third and final criterion involves the relationship between the mean time between collisions with neutral atoms (τ) and the plasma oscillation frequency (ω). If the plasma oscillation frequency exceeds the inverse of the collision time ($\omega\tau \gg 1$), the system exhibits fluid-like behavior rather than plasma behavior. This criterion ensures that collective interactions dominate over collisional effects, as required for plasmas.

$$\tau\omega > 1 \tag{2.4}$$

2.1.4 Plasma Classification: Thermal vs. Non-Thermal

Plasmas can also be categorized based on their thermodynamic equilibrium states, which are classified as hot (thermal) and cold (non-thermal). Hot plasmas represent high-energy systems in which electrons, ions, and neutral particles share comparable temperatures, achieving Local Thermodynamic Equilibrium (LTE). These plasmas are prevalent in fusion reactors and astrophysical environments. In contrast, cold plasmas exist in a state of thermal disequilibrium, where the electron temperature (T_e) significantly exceeds the temperatures of ions (T_i) and neutral gas (T_g), following the relationship $T_e >> T_i >> T_g$ (Wasa and Hayakawa, 1992).

The EPS discussed in this work primarily utilize cold plasmas due to their advantageous temperature properties. These properties not only prevent component degradation but also enable efficient charged-particle acceleration. The condition $T_e >> T_i$ enhances conductivity and facilitates stable ionization, both of which are critical for thruster operation (Hamrang, 2014).

While the simulations conducted in this study do not directly analyze particle temperatures, understanding their impact is essential for future research. Before delving into the specifics of the thruster, it is necessary to first examine the interaction between electric and magnetic fields to provide a comprehensive understanding of thruster functionality.

3 Propulsion state of art

Regarding thrusters, the development of these systems focuses on providing power to an engine to generate a force known as thrust. Different types of thrusters employ various methods to produce thrust; for example, chemical thrusters heat and expand gas through a nozzle. Electric thrusters, which are the focus of this thesis, primarily accelerate gases using either electrical heating or magnetic forces (Goebel et al., 2023). These thrusters are characterized by their low propellant consumption, a highly desirable feature in space system development. This efficiency significantly reduces the launch mass of satellites, leading to lower project costs (Sabale and Adams, 2024).

3.1 Propulsion systems

Propulsion technology has reached higher standards with the miniaturization of spacecraft systems (Yeo et al., 2020) (Radu et al., 2018) (Smith and Bae, 2023). This chapter, however, focuses on analyzing the engineering parameters and the most commonly used propulsion systems for spacecraft maneuvers: electric and chemical propulsion.

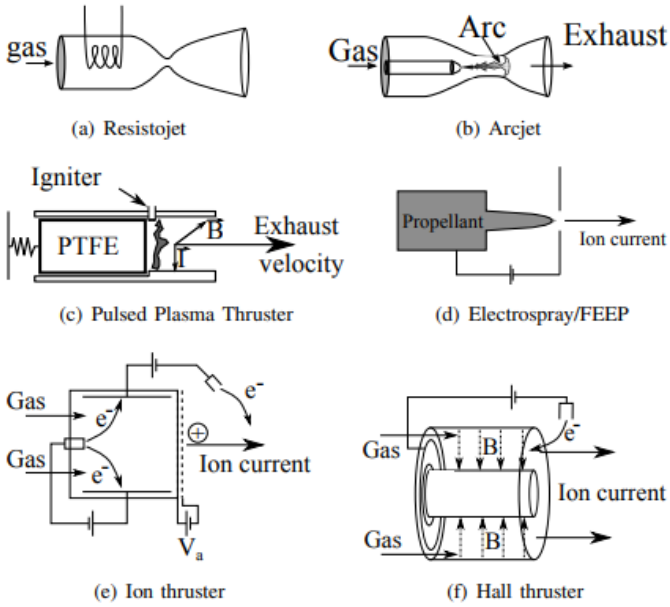

Figure 3.1. Schematic of electric thrusters. Source: Krejci and Lozano (2018)

3.1.1 Electric Propulsion System (EPS)

Electric thrusters are classified based on the acceleration method used to generate thrust. These systems employ electric or magnetic fields to alter the velocities of exhaust particles. Such technologies have been extensively tested and developed by universities and research programs, including the mini Helicon Thruster at the Massachusetts Institute of Technology (Batishchev, 2009) and the Helicon Double Layer Thruster (HDLT) at the Australian National University (Charles and Boswell, 2003).

Figure 3.1 presents examples of commonly used EPS in spacecraft. Each system is designed based on its ion acceleration mechanism, with its efficiency tailored to meet specific mission requirements. These systems are briefly described below (Goebel et al., 2023):

- Resistojet thrusters utilize an electric resistor to heat a non-reactive gas, which is then directed through a nozzle to produce thrust. They are simple and efficient, making them ideal for low-thrust applications.
- Arcjets employ an electric arc to heat the propellant gas, increasing its exhaust velocity and improving efficiency compared to chemical propulsion systems.
- Pulsed Plasma Thrusters ablate solid propellant using an electric arc, generating plasma that is accelerated electromagnetically. These thrusters are particularly suited for low-thrust, high-precision applications.
- Electrospray thrusters use conductive liquid propellants and high electric fields to generate and accelerate charged particles, enabling precise thrust control.
- Ion thrusters ionize neutral gas and accelerate ions electrostatically or electromagnetically, achieving high specific impulse with low thrust.
- Hall thrusters combine electric and magnetic fields to accelerate ions, providing efficient propulsion for a wide range of satellite missions.

3.1.2 Chemical Propulsion System (CPS)

As for Chemical Propulsion System (CPS), these generate thrust by accelerating a compressed fluid into a high-velocity exhaust stream, as illustrated in Figure 3.2. They utilize a converging-diverging nozzle geometry to compress and expand the gases. While the release of gas follows the same principle using a bell-shaped nozzle, the systems differ in their methods of energy release (Krejci and Lozano, 2018). These systems are also briefly described below:

- Cold gas thrusters utilize pressurized gas stored in a tank, which is expelled through a nozzle to generate thrust. These systems are simple, safe, and reliable but exhibit low efficiency and specific impulse.
- Warm gas thrusters heat the propellant before expelling it through the nozzle, enhancing both thrust and specific impulse compared to cold gas systems.

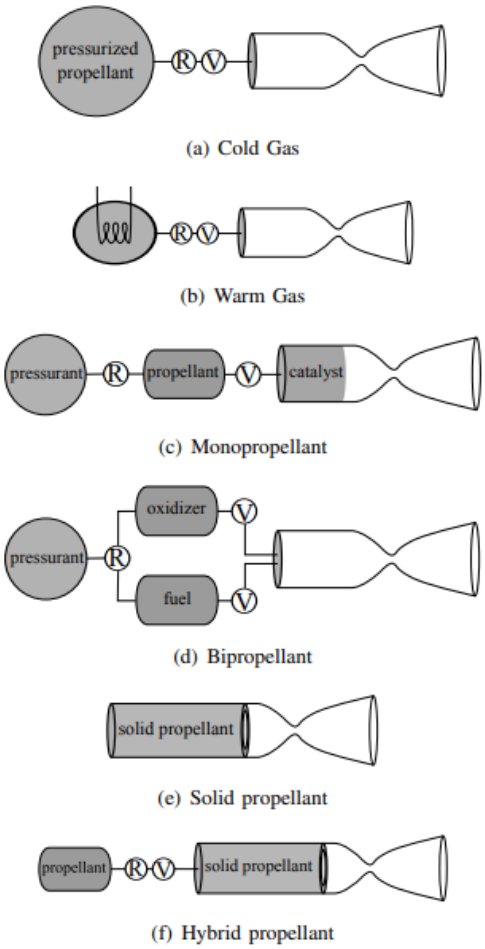

Figure 3.2. Schematic of chemical trhusters. Source: (Krejci and Lozano, 2018)

- Monopropellant thrusters use a single propellant that decomposes exothermically upon contact with a catalyst. The resulting gases are expelled through a nozzle to produce thrust.
- Bipropellant systems combine fuel and oxidizer, which react chemically to generate high-energy combustion gases. These gases are expelled through a nozzle, providing efficient thrust generation.
- Solid propellant systems use solid fuel that burns within the combustion chamber to produce thrust. However, they lack the ability to throttle or restart once ignited.
- Hybrid propulsion systems combine solid fuel with a liquid or gaseous oxidizer. This configuration allows for throttling and restarting while retaining advantages from both solid and liquid propulsion systems.

These systems will be compared in the following sections, focusing on engineering parameters to facilitate comparisons and assess their suitability for in-space applications.

3.2 Engineering parameters

EPSs have become critical for modern spacecraft due to high specific impulse and efficiency compared to the standard chemical propulsion. The engineering parameters define performance, operational limits and suitability for specific missions. This section will explain some parameters important to an electric thruster and also to the APT model.

3.2.1 Thrust

One of the main engineering parameters for engines is the T, which can be defined as a rate of change of momentum during propellant consumption. this phenomena is define by particles leaving the engine at v_z, with a mass flow rate, $\dot{m}_p$ (Goebel et al., 2023).

$$T = \frac{\partial}{\partial t}\left(m_p v_{ex}\right) \tag{3.1}$$

For EPS, the particles accelerated are ions and electrons reaching high exhaust velocities. Considering the respective mass of ions being exhausted, they outreach any other particle being propelled, as for electrons for instance. Therefore the thrust equation is a function that depends on the ion mass flow,$\dot{m}_i$, and ions exhaust velocity, $v_{ex,i}$.

$$T \approx \dot{m}_i v_{ex,i} \tag{3.2}$$

This equation is the basic form for thrusting measurements and shall be adapted to each type of thrust method. For this work, the numerical method will be explained with the PIC code.

3.2.2 Specific Impulse

As a measure of thruster efficiency, the I_{sp} is defined as the ratio of thrust to the rate of mass flow ($\dot{m}_p$) or the propellant consumed during the process. It is expressed in seconds.

$$Isp = \frac{T}{\dot{m_p} g_0} \tag{3.3}$$

where g_0 represents the standard gravitational acceleration, $9.81, \mathrm{m/s^2}$. For mathematical simplification, the I_{sp} can be redefined using Equation 3.2.

$$Isp = \frac{v_{ex}}{g_0} \tag{3.4}$$

A higher specific impulse (I_{sp}) indicates greater fuel efficiency, allowing for more significant changes in velocity (ΔV) with a considerable reduction in propellant mass. Before comparing specific impulse and thrust, the concept of velocity change (ΔV) is briefly reviewed to enhance

the analysis.

3.2.3 Delta-V

The change in velocity, commonly referred to as Delta-V, ΔV, is a fundamental concept in spacecraft propulsion (Leomanni et al., 2017). During mission planning, it serves as a critical parameter for determining the spacecraft's capability to perform maneuvers such as orbital insertion, station-keeping, interplanetary transfers, or de-orbiting (Zanola, 2019).

$$\Delta V = I_{sp} \cdot g_0 \cdot ln\left(\frac{m_{initial}}{m_{final}}\right) \tag{3.5}$$

where $m_{initial}$ and m_{final} represent the spacecraft's initial and final masses, respectively. Equation 3.5 quantifies the "maneuverability" of a spacecraft based on the designed propulsion system and the available propellant. Table 3.1 highlights differences in applications, aiding in trade-off analysis for propulsion system selection.

Table 3.1. Delta-V ΔV mission comparison

Mission type	Typical ΔV requirement	Propulsion System Preference
LEO to GEO Transfer	$\sim$ 3-4 km/s	Chemical (high thrust needed)
Station-Keeping (GEO)	$\sim 50 m/s/year$	Electric (efficient long-term operation)
Mars Transfer	$\sim$ 5-6 km/s	Electric or hybrid
Deep-Space Exploration	$> 10 km/s$	Electric

To achieve high values of ΔV, it is essential to consider efficient propulsion systems along with a careful mass management. With the concept of Delta-V addressed the discussion will continue to understand the relation between specific impulse and thrust.

3.2.4 Specific Impulse and Thrust implications

The difference in I_{sp} between chemical and electric propulsion systems highlights their respective strengths and limitations. Chemical thrusters are designed to produce high thrust levels, which are essential for overcoming planetary gravity or executing rapid trajectory changes. The method of thrust generation and the associated I_{sp} significantly differentiate chemical thrusters from electric thrusters.

As shown in Figure 3.3, EPSs achieve much higher specific impulses, typically ranging from 1,000 to 10,000 seconds. This is attributed to the use of external electrical energy to accelerate propellant ions to extremely high velocities. For example, HET commonly operate with I_{sp} values between 1,500 and 3,000 seconds.

Despite the high thrust levels offered by chemical thrusters, they require substantial propellant consumption due to their relatively low I_{sp}. For instance, launching a satellite into Geostationary Orbit (GEO) using chemical propulsion demands several tons of propellant to achieve the necessary ΔV. A typical Geostationary Transfer Orbirt (GTO) mission requires

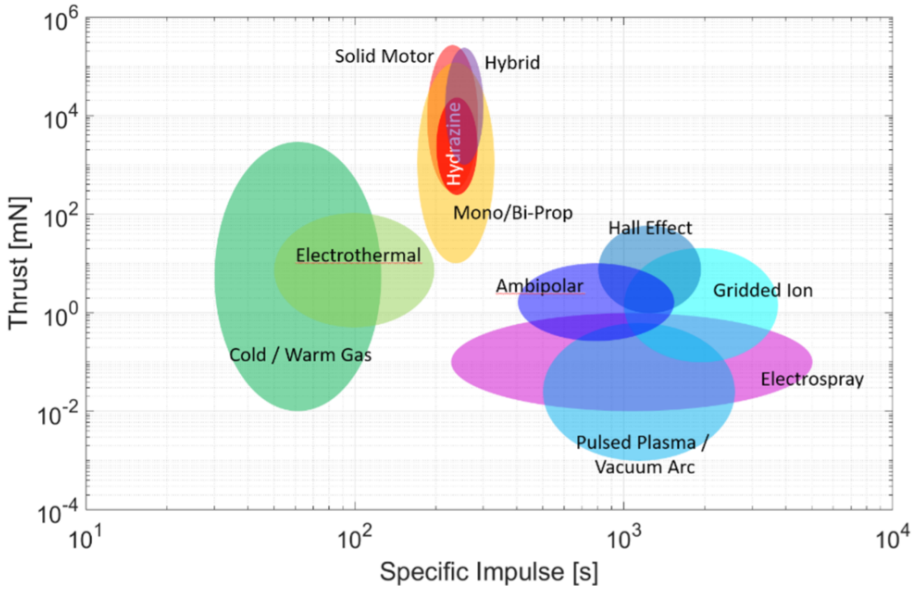

Figure 3.3. Specific impulse and thrust comparison for different propulsion methods. Source: (NASA Small Spacecraft Systems Virtual Institute, 2025)

Table 3.2. Isp impact comparison

Parameter	Chemical Propulsion	Electric Propulsion
Specific Impulse (s)	200 - 500	1000 - 10000
Thrust (N)	10^3 - 10^7	10^4 - 1
Mission application	Launch, rapid maneuvers	Station-keeping, deep space
Propellant mass (kg)	High (tons)	Low (grams to kilograms)

a ΔV of approximately 3–4 km/s to transition from Low Earth Orbit (LEO) to GEO. When chemical propulsion is used, this maneuver results in a high propellant mass fraction, often exceeding 80% of the spacecraft's initial mass (NASA Small Spacecraft Systems Virtual Institute, 2025).

Specific impulse serves as a fundamental metric for comparing propulsion systems by quantifying their efficiency in propellant mass utilization. The selection between these systems is governed by mission-specific requirements, including thrust levels, power availability, and the required velocity change, ΔV. Trade-off studies represent the formal methodology for determining the most appropriate propulsion system, emphasizing the complementary roles that different systems may fulfill within the mission profile.

3.3 EPS missions

As the development of miniaturized spacecraft has progressed, many of these systems now perform both service-providing and scientific missions. The advent of propulsion miniaturization has significantly expanded the capabilities and operational range of small spacecraft. According to Zanola (2019), electric propulsion is expected to become the preferred choice for space missions. Some types of missions are outlined below.

The first method for changing altitude involves providing acceleration either in the direction of the spacecraft's velocity or opposite to it. A relatively inexpensive maneuver, considering its direct relationship with ΔV and velocity, is the inclination change. This maneuver consists of applying thrust perpendicular to the current orbital plane.

One of the primary missions for small spacecraft is orbit maintenance, which ensures that the system remains on its intended orbital path despite external interferences or perturbations, such as atmospheric drag. Failure to maintain orbit can lead to a reduced lifespan for the spacecraft and premature reentry. Implementing an EPS can significantly extend the expected mission duration by mitigating these effects.

Mission Analysis for Electric Thrusters (2019)

EPS / Mission	HPT	ECR thruster	PPT	Electrospray/ FEEP	Ion thruster	Hall thruster	electro thermal thruster
LEO in plane manoeuvre	🟢	🟡	🔶	🟢	🟢	🟢	🟡
LEO to GEO	🔴	🔴	🔴	🔶	🟢	🟢	🔴
LEO plane change	🟡	🟡	🔴	🔶	🟢	🟢	🔴
High Orbit plane change	🟢	🟡	🔴	🟢	🟢	🟢	🔴
Moon and NEOs mission	🔴	🔴	🔴	🔶	🟢	🟢	🔴
Orbit maintenance	🟢	🟡	🔶	🟢	🟢	🟢	🟡
Formation Flight	🟢	🟡	🟢	🟢	🟢	🟢	🟢
Inspection	🟢	🟡	🟢	🔴	🔴	🔴	🟢
Attitude Control and Desaturation	🔴	🔴	🟢	🔶	🔴	🔴	🟢

Legend	
🟢	Suitable with current technology
🟡	Probably suitable in a few years
🔴	Not suitable in the foreseen future
🔶	Suitable if extended tank is possible

Figure 3.4. Generated mesh, the injection area to exhaust are respectively from left to right. Source Zanola (2019)

As illustrated in Figure 4.1, an extensive investigation has been conducted on the application of propulsion systems across various CS missions. The HPT propulsion system demonstrates significant potential for success in LEO in-plane maneuvers, high orbit plane changes, orbit maintenance, formation flight, and inspection missions. As a result of this thesis, the simulation output variables will be utilized to evaluate these performances using orbital dynamics software such as STK Agile.

4 Ambipolar Thruster

Among the various configurations for electric thrusters, this thesis proposes a simulation of an APT, a model currently under development at the LPF-UnB Miranda et al. (2019). APTs generate thrust by ionizing the injected gas, typically Argon or Xenon, into an ambipolar plasma coupled with a magnetic field. The plasma is then axially accelerated using a magnetic nozzle.

Two widely recognized types of APTs are the HPT, which employs high-density plasma, and the Electron Cyclotron Resonance Thruster (ECRT), which utilizes resonance heating Wachs and Jorns (2021). Despite their differences, both systems rely on the same principle of Radiofrequency (RF) waves and a magnetic nozzle for plasma acceleration. The design adopted in this work is based on the principles of HPT and may be adapted for other variations.

4.1 Configuration

The thruster consists of a feeding system that injects gas into the dielectric chamber, an RF antenna surrounding the chamber, and a set of permanent magnets that create a magnetic field along the system's axis, as will be further examined in Chapter 6. Compared to other electric propulsion systems, the HPT offers several advantages, such as eliminating the need for a cathode to neutralize the exhaust plume. This absence of electrodes prevents erosion, thereby significantly increasing the thruster's lifespan.

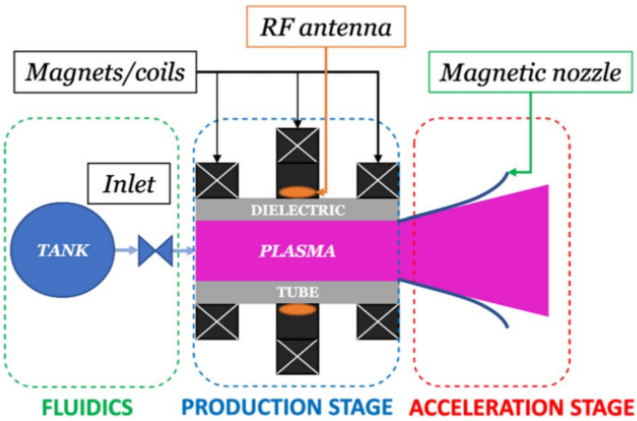

Figure 4.1. Design of an HPT . Source: van Lynden (2023)

There are two primary stages to consider within the thruster: the ionization of gas inside the chamber and the acceleration of particles through the magnetic nozzle. This process results in a high-density plasma with low power consumption. The ionized gas is confined by the magnetic

field within the chamber and then expands along the axis, guided by the magnetic nozzle.

4.2 Ionization and acceleration

4.2.1 Ionization

HPTs generate plasma through a wave-based ionization method. This ionization occurs in a dielectric tube where the propellant gas is injected (Squire et al., 2003) (Kuwahara et al., 2016). The components involved in ionization are the following:

- A helical RF antenna around the chamber.
- Magnetic field generated by magnets.
- Neutral gas as a propellant

Therefore, the ionization process starts with the RF antenna generating helicon waves that propagate through the magnetized plasma (Ahedo, 2013). These waves transfer energy to electrons in the gas, colliding with neutral atoms and than causing ionization, whereas the energy absorption mechanism is described below.

$$P_{abs} = \frac{1}{2}\int_V \mathbf{j}\cdot\mathbf{E}^* dV = \frac{1}{2}\int_V \sigma_{eff}|\mathbf{E}|^2 dV \tag{4.1}$$

where P_{abs} is the absorbed power, $\mathbf{j}$ is the current density, $\mathbf{E}^*$ is the complex conjugate of the electric field, and σ_{eff} is the effective conductivity tensor of the plasma (Iannarelli et al., 2024). The ionization rate depends on electron temperature and neutral density:

$$\frac{dn_i}{dt} = n_e n_n \langle \sigma_i v_e \rangle \tag{4.2}$$

where n_e is electron density, n_n is neutral density, and $\langle \sigma_i v_e \rangle$ represents the ionization rate coefficient (Iannarelli et al., 2024).

4.2.2 Magnetic nozzle and acceleration mechanism

The magnetic nozzle is a convergent-divergent magnetic field created by a set of magnets, which confine, expand, and accelerate the plasma as it exits the chamber, following the magnetic field lines. This phenomenon is analogous to the physical bell-shaped nozzle commonly used in chemical thrusters, where fluid expansion due to pressure interacts with the nozzle walls. In the magnetic nozzle, the plasma undergoes a sonic transition at the minimum cross-sectional area, referred to as the magnetic throat, and expands supersonically in the divergent section, mimicking the behavior of a neutral gas expanding in a physical nozzle (Merino, 2013).

Mathematically we can describe the conversion of electron thermal energy into ion kinetic

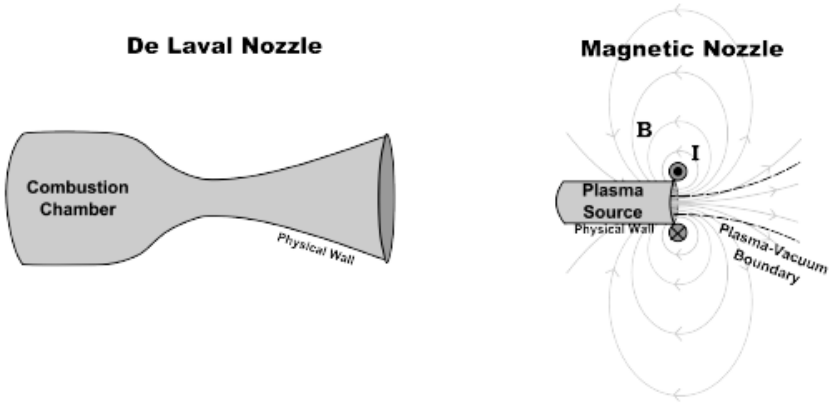

Figure 4.2. Comparison between de Lava nozzle and magnetic nozzle. Source: Ebersohn et al. (2014)

energy through and ambipolar field (Navarro-Cavallé et al., 2019). It arises from a electron pressure gradient:

$$e\mathbf{E} = -\frac{\nabla p_e}{n_e} \tag{4.3}$$

where e is elementary charge, $\mathbf{E}$ is the electric field, and p_e is the electron pressure (Navarro-Cavallé et al., 2019)(Ahedo, 2013).

The ions, being less magnetized than electrons, are accelerated by this electric field. The momentum equation for ions can be written as:

$$m_i n_i (\mathbf{u}_i \cdot \nabla)\mathbf{u}_i = e n_i \mathbf{E} - \nabla p_i \tag{4.4}$$

where m_i is ion mass, n_i is ion density, $\mathbf{u}_i$ is ion velocity, and p_i is ion pressure.

The magnetic nozzle converts thermal energy to directed kinetic energy through:

$$\frac{1}{2} m_i u_i^2 \approx T_e \tag{4.5}$$

In this process, electrons are primarily magnetized (following magnetic field lines), while ions are typically less magnetized. This creates an electric field that accelerates ions and decelerates electrons to maintain quasi-neutrality (Ahedo, 2013). The diverging magnetic field lines in the nozzle region cause the plasma to expand and accelerate, similar to gas expansion in conventional nozzles, but with the critical advantage of avoiding wall erosion (Williams and Walker, 2015).

The absence of physical walls ensures that these forces effectively prevent plasma-wall interaction, thereby eliminating erosion. Thrust is generated from the momentum of the plasma flow, which is created through ionization within the chamber and subsequent acceleration via the magnetic nozzle (York et al., 1992).

4.3 Miniaturization set up

The HPT system has been studied at the LPF - UnB since 2019 (Miranda et al., 2019). The project originated as an experimental test bench engine , figure 4.3, featuring a 1.5m long dielectric tube and two sets of coils, designed both to validate the propulsion system and to serve educational purposes by training students in electric propulsion applications.

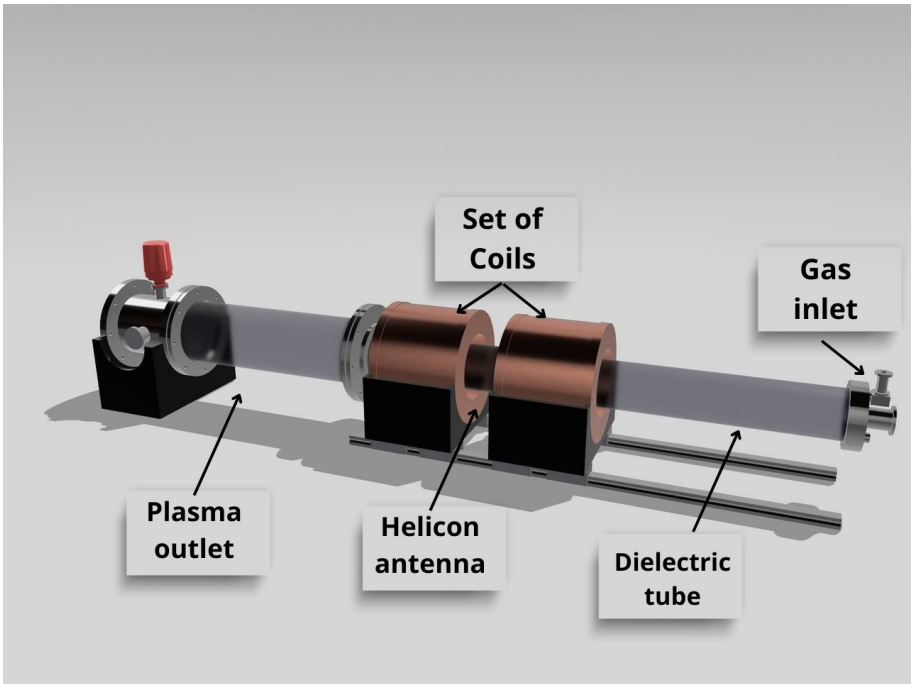

Figure 4.3. HPT Test bench model at the LP-UnB.

After further investment, the laboratory has begun developing a CubeSat version of this test bench (Miranda et al., 2019), as shown in Figure 4.4. The experiment is being conducted alongside numerical simulations. However, it presents significant challenges, as a CS propulsion system is considered a subsystem and involves greater complexity in integration with other subsystems and the payload.

The model proposed in this thesis is based on PQ constraints, with dimensions of 50 x 50 x 50 mm. This model represents a preliminary design and serves as the foundation for the development of the payload system, specifically the propulsion system. It includes two sets of magnets, a gas inlet, an antenna, an ionization chamber, and a nozzle.

Although this propulsion system does not inherently require a physical nozzle due to the magnetic nozzle created by the applied magnetic field, testing has shown that incorporating a physical nozzle aids in directing ions and can increase particle velocities when designed to align with magnetic field lines, thereby avoiding wall contact.

The antenna is not represented in this work due to limitations in plasma source rate modeling, as explained in Section 5. However, it remains a critical component of the system, and further simulations are required to account for the interaction between ionization and the antenna. Similarly, the gas inlet is another section of the system that is not considered in this

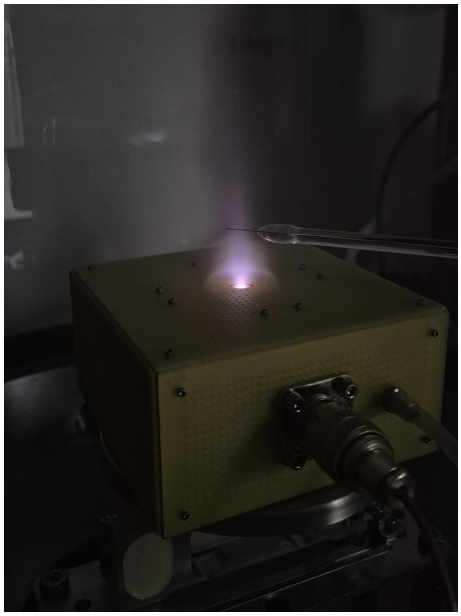

Figure 4.4. CubeSat Ambipolar Thruster developed at LPF-UnB is an experimental propulsion module with dimensions of 100 x 100 x 50 mm.

simulation. Table 4.1 provides details of the dimensions used in the numerical simulation and figure 4.1 represents the 3D model of the designed PQ.

Table 4.1. Initial thruster constrains

Part of the system	Dimension
Circular magnets	35 mm in diameter
Ionization chamber	10 mm diameter with 5mm compriment
Nozzle section	10 mm to 5mm diameter with 10 mm compriment

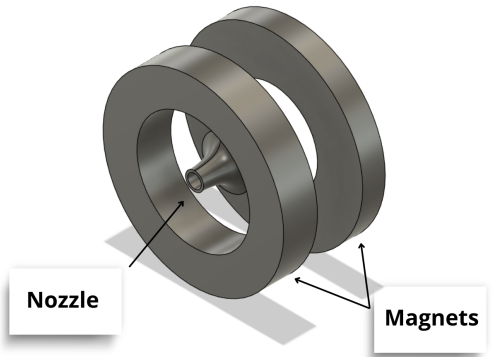

Figure 4.5. PocketQube Ambipolar Thruster model to be simulated.

5 Computational simulation

The computational thruster simulation incorporates two principal methodologies: initially, the magnetic nozzle modeling, which creates and evaluates the magnetic field lines in both radial and axial orientations throughout the thruster. Subsequently, once the magnetic field values are established, the thruster geometry is integrated into the PIC code, which has been formulated to analyze particle motion and dynamics within the system.

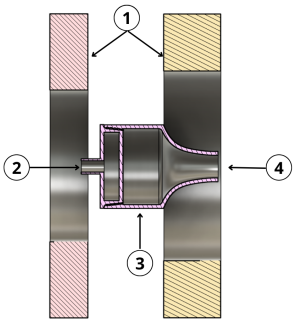

Figure 5.1. Sliced view of the propulsion system. Legend: 1 - Magnets, 2 - Gas inlet, 3 - Ionization chamber, 4 - Nozzle

The simulation domain, illustrated in Figure 5.1 and 5.2, focuses on the upper half of a cross-section of the APT, leveraging its symmetry. The delimited rectangle indicates the region where the X-Windows Object-Oriented Particle-in-Cell (XOOPIC) code simulation will be conducted, taking into account the magnetic influence. This approach is adopted to optimize computational efficiency and reduce simulation time.

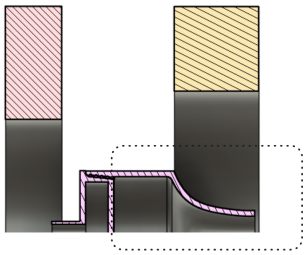

Figure 5.2. Thruster simulation domain.

5.1 Finite element Method Magnetics FEMM

The magnetic nozzle, created by the permanent magnets, is responsible for accelerating particles to generate thrust while preventing wall interaction. To model the magnetic field lines, the FEMM software has been selected. This software is widely used for solving 2D electromagnetic problems in low-frequency systems.

The simulation process is divided into the following:

- Geometry set up
- Boundary conditions
- Mesh generation
- Output (field lines and magnetic values)

5.1.1 Geometry

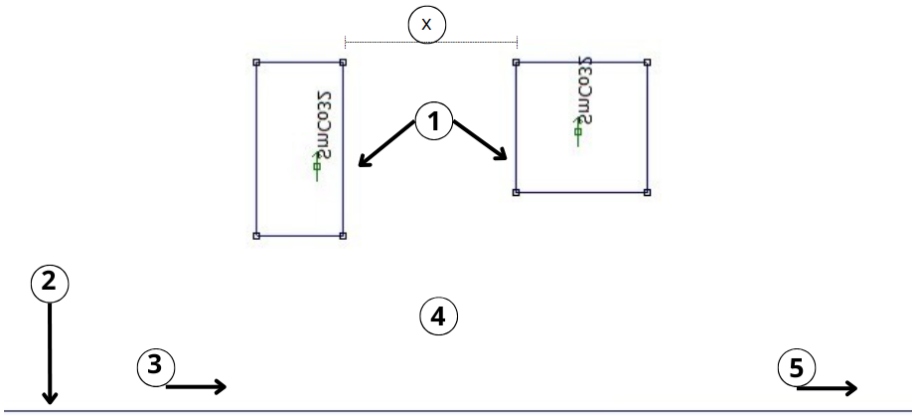

Figure 5.3. Geometry inserted in the FEMM software, the plasma injection area to exhaust are respectively from left to right.Legend: "x" variable defines the dimensions to be tested in table 5.1, 1 - Magnets, 2 - Axis of simulation, 3 - Gas inlet, 4 - Ionization chamber region, 5 - Nozzle.

The first step of the simulation involves positioning the magnets near the thruster axis. The geometry is configured as shown in Figure 5.3. One of the objectives of this thesis is to investigate the effects of varying the distance between the magnets. The values presented in Table 5.1 represent experimental parameters. As part of the miniaturization process, it was decided to increase the distance between the magnets to observe its numerical impact and, subsequently, validate these findings through experimental testing.

The chosen geometry of the magnets is arbitrary and might be investigated in further research. The actual work will only investigate the distance interference, considering the PQ constraints. All configurations are shown below.

Table 5.1. Magnets distance configuration, x

Configuration	Distance (mm)
1	10
2	11
3	12

5.1.2 Boundary conditions and mesh

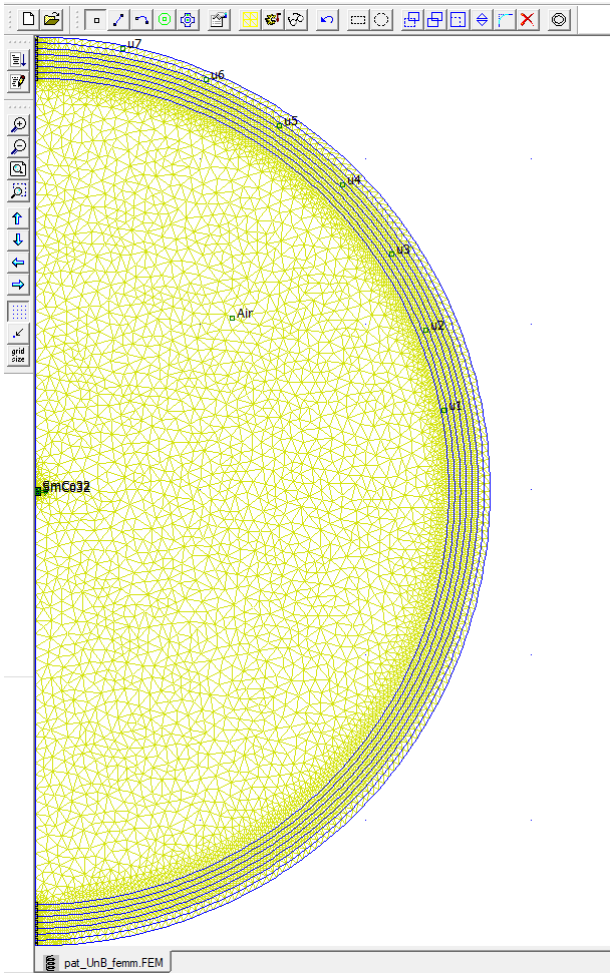

Figure 5.4. Generated mesh with boundary lines.

The boundary conditions are a critical aspect of defining the limits of the simulation. First, the magnets are configured to the desired values. The external boundary is placed sufficiently far from the system to prevent interference when generating the magnetic field lines.

The mesh, shown in Figures 5.4 and 5.5, is used to solve magnetic equations in small regions. The resolution and efficiency of the simulation are directly related to the size of these regions. However, an excessively fine mesh can lead to an overwhelming number of regions, causing the computation time to exceed acceptable limits. FEMM employs a discretization method using triangular elements and approximates the solution by interpolating potential values at each vertex of the triangles.

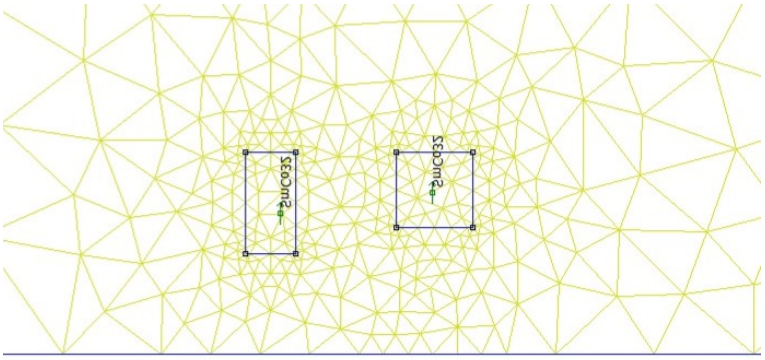

Figure 5.5. Generated mesh, the injection area to exhaust are respectively from left to right.

The output files from FEMM are then directly uploaded into the PIC code, which uses the magnetic field lines to simulate particle interactions.

5.2 Particle-in-cell model

The two-dimensional model of the APT is formulated using cylindrical coordinates, focusing on the (z, r) coordinates while neglecting variations along the azimuthal direction. The interaction between plasma particles and magnetic field lines is simulated using the XOOPIC in Musso et al. (2007). In this computational approach, the positions and velocities of charged particles are determined by solving the equations of motion under the influence of electric and magnetic fields:

$$\frac{d\mathbf{r}}{dt} = \mathbf{v} \tag{5.1}$$

$$m\frac{d\mathbf{v}}{dt} = q(\mathbf{E} + \mathbf{v} \times \mathbf{B}) \tag{5.2}$$

The charge density is subsequently discretized onto a spatial grid through a weighting process, enabling the solution of Poisson's equation to derive updated values of electric potential and electric field:

$$\nabla^2\phi = -\frac{\rho}{\varepsilon_0} \tag{5.3}$$

$$\mathbf{E} = -\nabla\phi \tag{5.4}$$

These fields are then incorporated into the particles' equations of motion, and the computational cycle iterates.

In this system, the axial axis of the engine is treated as an axis of symmetry, permitting analysis of only its upper half. The grey regions represent the thruster walls, which are modeled

as electrical conductors. The PIC model employed does not directly simulate the gas ionization process; therefore, as proposed by Musso et al. (2007), a designated region (depicted in pink) represents the gas ionization produced by the antenna. In this region, argon ions and electrons are directly introduced into the computational domain at a specified plasma rate. The Monte-Carlo collision model governs the ionization conditions resulting from interactions between electrons and argon gas, which generate the argon ions. The gas pressure within the tube is maintained at 5×10^{-5} torr.

The spatial grid employed for plasma feature discretization consists of a 1024×128 mesh, which provides sufficient resolution for accurate plasma representation while remaining computationally tractable.

Modeling all individual particles in the plasma would render the computational requirements prohibitively demanding. Due to the significant particle production in the system, a common approach in PIC simulations is employed: the definition of superparticles, each representing a "cloud" or ensemble of electrons or ions. The position of each superparticle corresponds to the center of mass of its respective cloud, while its velocity represents the cloud's average velocity. This approach substantially reduces the number of tracked particles and, consequently, the computational execution time. In this simulation, each superparticle represents 10^5 actual particles. For simplicity, these superparticles are referred to as "particles" throughout this research.

Following Musso et al. (2007), plasma source rate values have been established based on experimental data. A systematic investigation was conducted to examine the influence of these parameters on plasma density and engineering values, thereby establishing a framework for future experimental studies.

6 Results

As described in the previous section 5.2, a 2D plasma and magnetic field interaction were defined to simulate the thruster for PQ constrains. This chapter will present and discuss the outputs from either FEMM and PIC model.

The PIC code does not simulate plasma ionization and therefore insert argon ions and electrons. The species are named, respectively, as ions1 and electrons and the collisions between ions and electrons generate a third specie, called ions2, but the values of ions2 are smaller compared to ions1, thus bein neglected due to low influenc on results.

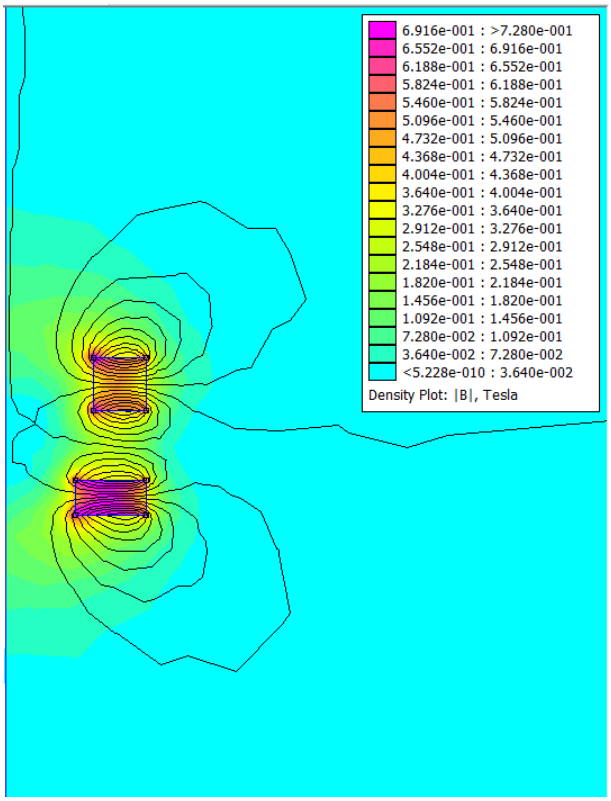

Figure 6.1. Configuration 1 - 10mm : Magnetic field (tesla) and magnetic lines

6.1 FEMM

The simulation of magnetic lines from FEMM were inserted into the X-Windows Object-Oriented Particle-in-Cell code (XOOPIC) code to generate the interactions of the plasma with the magnetic field applied. The different configurations tested are ment to verify how the design

could affect the particles exhaust without compromising the PQ constrains.

6.1.1 Magnetic field and magnetic lines

The first designed configuration was set to understand, preliminary, how the simulation would behave. The left part of figure 6.1 show the axis of the thruster and the direction of particles start form the bottom magnet.

The proposed configuration has two difference sizes of magnets. These magnets has different purposes, the inlet magnet is closer to the system. The objective to position the magnet this close to the thruster is to avoid plasma reflux. It has a function to prevent the plasma to follow an undesired flow against the gas inlet. Therefore the second magnet is positioned to direction the particles into the exhaust direction, assuring the particles do not accumulate inside the chamber and avoiding the reflux.

The high intensity pink color shows that the inlet magnet has a higher magnetic field. The magnetic lines in this simulation are not following a homogeneous path, this might lead to an undesired flow of particles.

6.1.2 Variation of distance between magnets

The variation of distance between the inlet magnet and the nozzle magnet are proposed to evaluate the electric potential response, which concerns to the path of electrons, and particles exhaust velocities. Then the values of specific impulse can be compared to select an ideal distance for further iteration of other components.

Furthermore, the direction of magnetization is investigated to validate the efficiency of magnetic lines for ions path, the table 6.1 presents the iteration numbers adopted for these simulations.

The values of magnetic field achieved are in table 6.1. The radial configuration in figure 6.1 shows a convergence of magnetic lines in the ionization chamber area, which is a good result as for the ionization process. As the particles pass through the ionization chamber, the longer they are under the influence of the antenna, the higher is the plasma density and thus increasing efficiency in the thruster. This assumption must be confirmed in the PIC simulation.

As for the inlet magnet, the simulations reached a high value of magnetic field around 0.7319 Tesla, see in Figure 6.1, right table. This intensity can prevent the plasma to follow the lines back to the gas inlet.

The second configuration, shown in figure 6.2, they are set with an axial direction, along the longitudinal axis of the thruster. In comparison to the radial configuration, the magnets in this scenario achieved a different magnetic field, as high as 0.625 Tesla. The intensity of the magnet is also changed, due to the direction of magnetic lines, the concentration is stronger on the face pointed to the center of the thruster.

Another observable difference is the intensity in each magnet, the nozzle magnet in this scenario presents higher values of magnetic field, which might bring higher exhaust velocities.

Regarding the magnet distance, the first experiment presented a higher magnetic field value for an radial profile. The axial simulation, however, had an decrease in the magnetic field. The analysis needs then the results from particles position, electric potential and particles exhaust velocity to create a consolidated hypothesis.

Table 6.1. Magnets configuration

Configuration	Distance (mm)	Magnetization direction
1	10	Radial
2	11	Axial and Radial
3	12	Axial and Radial

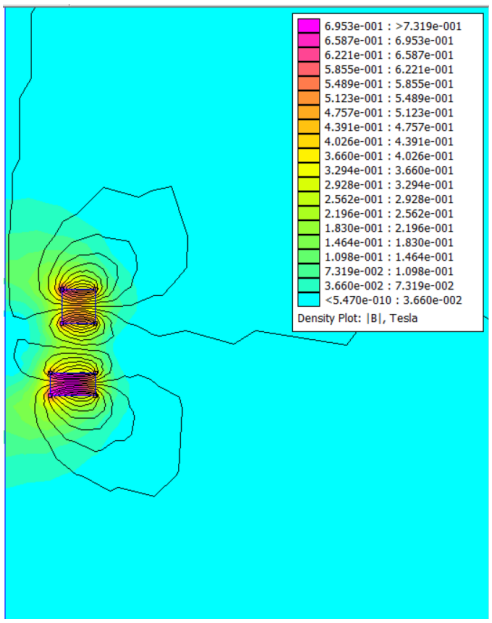

Figure 6.2. Radial Magnetization for 11mm.

6.2 XOOPIC

The simulation method proposed in this theses did not compute the ionization of particles, therefore they were inserted in the plasma source with a suggested variable given by Musso et al. (2007). The simulation was conducted into two different variables:

- The plasma generation with a source rate, experimental value proposed by Musso et al. (2007);
- The distance from the two magnets and its magnetization direction.

6.2.1 Plasma source rate analysis

Musso et al. (2007) suggested a value of plasma source rate, which comes from an exper-

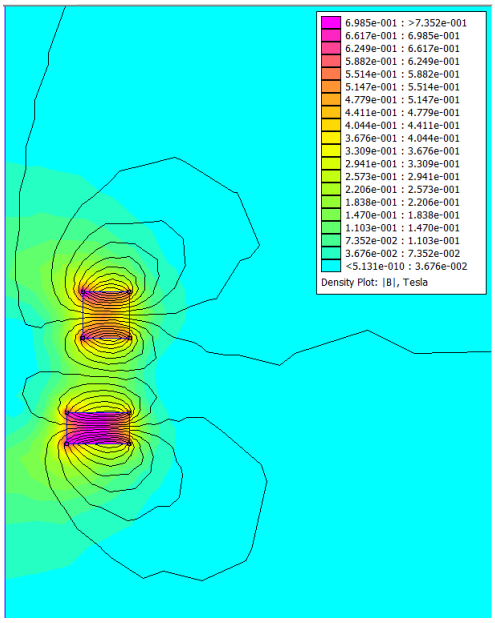

Figure 6.3. Radial Magnetization for 12mm.

imental value in laboratory. This value represents the insert of ionized particles at a specific rate ($s^{-1}m^{-3}$). As the diagnosis methods in the LPF-UnB are improving, it has been evaluated three parameters resultants from the generation of plasma in order to understand efficiency of the design and the interferences that might arise. This section analyses the figures into electric potential, particles position and particles velocities.

- Electric potential

The electric potential is a parameter that allows to understand the behave of electrons and wall interactions. Figures 6.6, 6.7 and 6.8 represent the electric potential simulated. The darker color shade represents high concentration of electrons.

Figure 6.6 has a desired behave, as the concentration of electrons is along the axis of the domain and increases.

The following figures, 6.7 and 6.8 show a significant spot of undesired electric particle concentration, this induces that the particles are moving towards the gas inltet.

A critical response to enhance of plasma rate is observed in figure 6.8. There are two focus of electric potential, aside from the desired in the axis. The first is a moderate concentration in the gas inlet, suggesting possible reflected ions or trapped electrons. The last interaction is a high potential in the nozzle physical wall, which might decrease particles velocities.

- Ions and electrons positions

Ions (yellow) and electrons (red) are presented in figures 6.9, 6.10 and 6.11. The first image has a expected position of electrons and ions, as electrons are lighter than ions, they tend to accumulate inside de chamber, therefore increasing the ion concentration in the chamber.

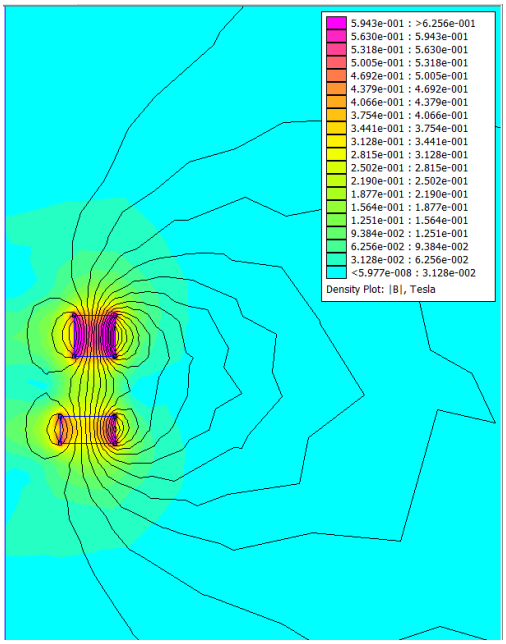

Figure 6.4. Radial Magnetization for 11mm.

As the plasma rate increases, the number of particles also increases. Nevertheless, figure 6.11, show an undesired amount of concentration of particles inside the ionization chamber, the number of electrons also increases along the axis, what might suggest high velocities inside the chamber and also exhausting the system.

- Particles velocity

The average values of exhaust velocities were computed in table ?? and were taken from $z > 0.014$, to better validate the efficiency of particles acceleration. These values are just taking ions into consideration. The values computed show an increase tendency in velocity, as a direct function of plasma density.

However, analyzing from points between $z > -0.012$ and $z < 0$ there is a high value of velocity in both figures 6.13 and 6.14, and a lower for figure 6.12. The values of velocity from figure 6.14 are also increasing, towards the plasma source, as high as they reach in the end of the domain.

Table 6.2. Ion velocities for plasma rate

Plasma rate	V_z (m/s)
10^{16}	2.3606e+03
10^{18}	3.3043e+03
10^{20}	4.37188e+03

After validation of plasma rate, the configurations of magnets were analyzed with the same parameters as electric potential, particles positions and particles exhaust velocities.

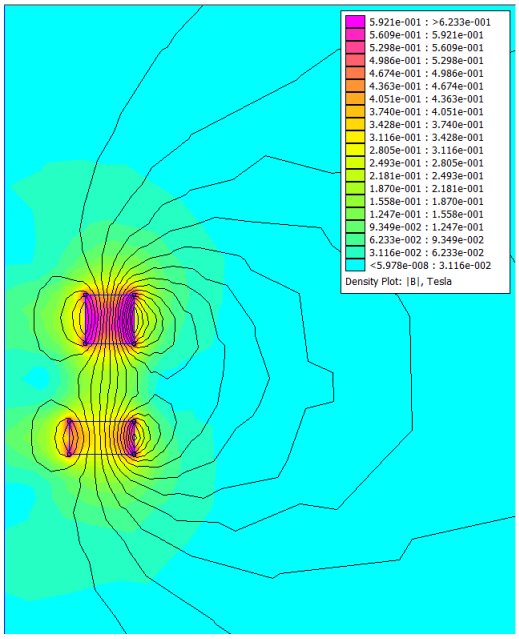

Figure 6.5. Radial Magnetization for 12mm.

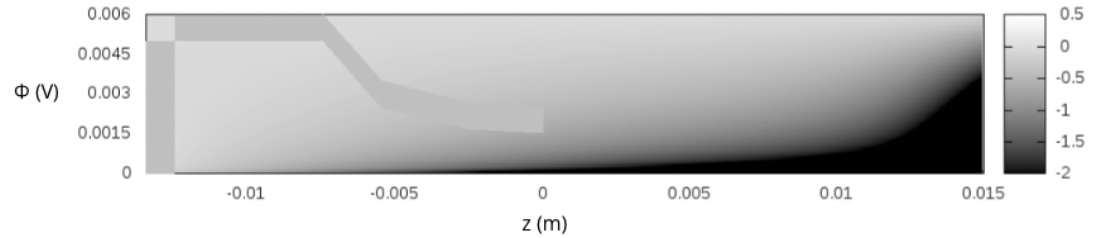

Figure 6.6. Electric potential with a 10^{16} plasma rate, configuration 1.

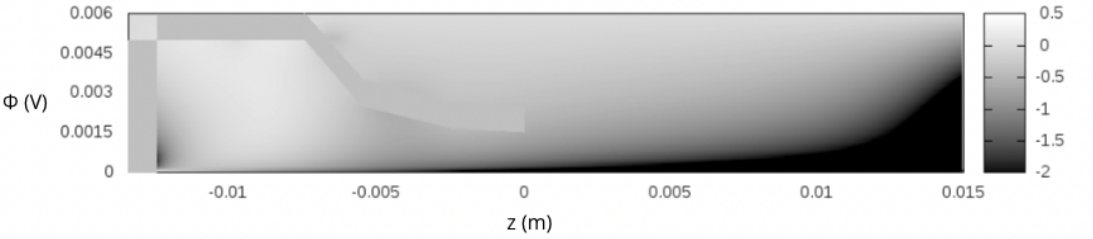

Figure 6.7. Electric potential with a 10^{18} plasma rate, configuration 1.

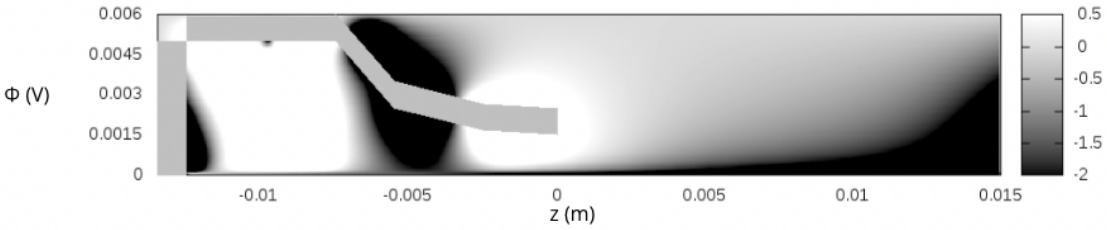

Figure 6.8. Electric potential with a 10^{20} plasma rate, configuration 1.

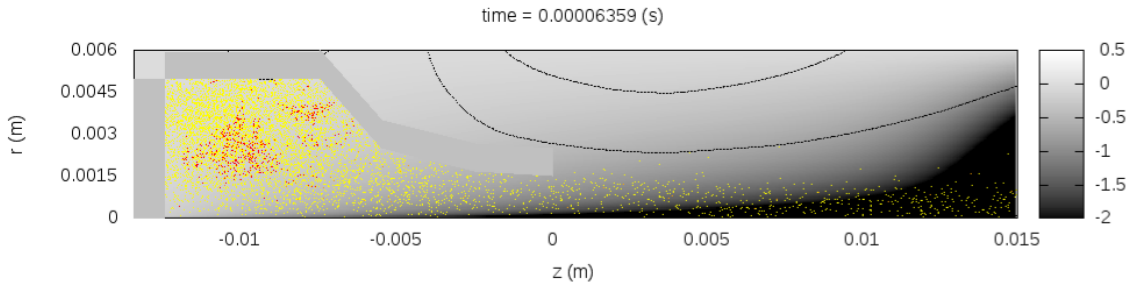

Figure 6.9. Ions and electrons position with a 10^{16} plasma rate

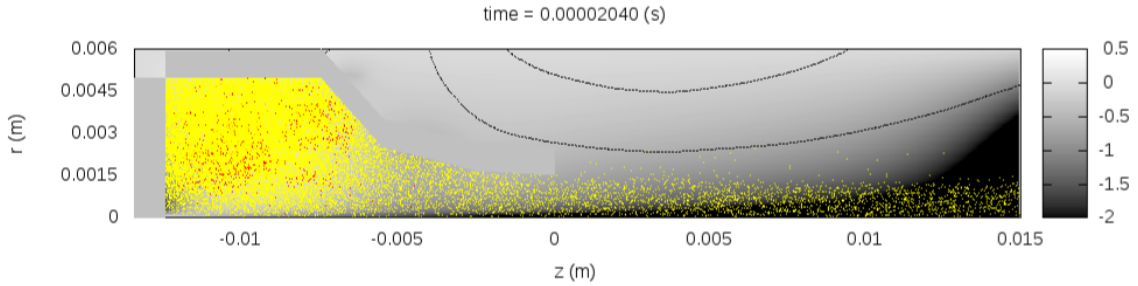

Figure 6.10. Ions and electrons position with a 10^{18} plasma rate

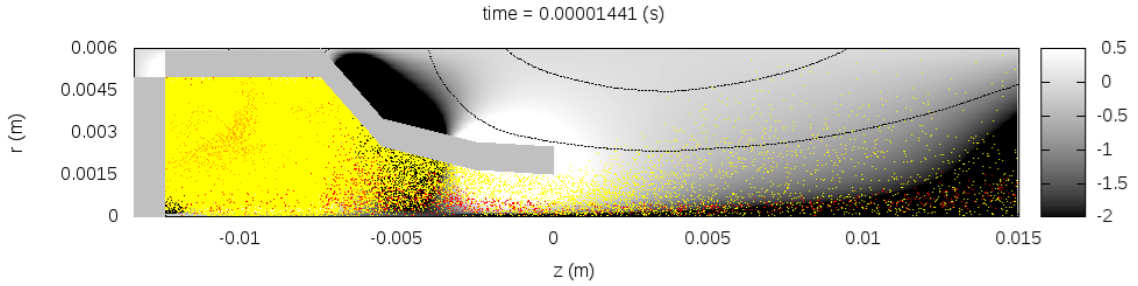

Figure 6.11. Ions and electrons position with a 10^{20} plasma rate

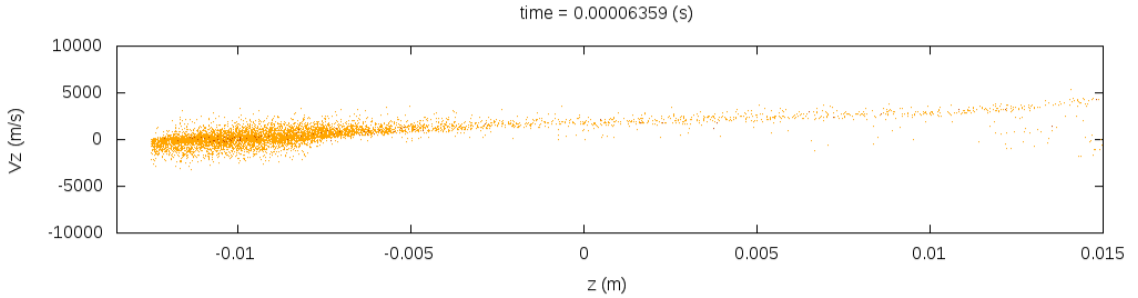

Figure 6.12. Particles velocity V_z with a 10^{16} plasma rate

6.2.2 Variation of distance and magnetization direction

From this point the simulations adopted the plasma rate of 10^{16}, which will be justified in the conclusion as a better parameter for the design presented.

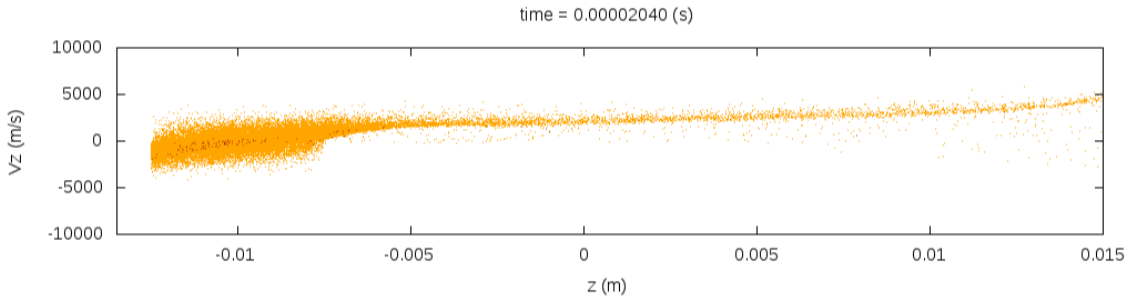

Figure 6.13. Particles velocity V_z with a 10^{18} plasma rate

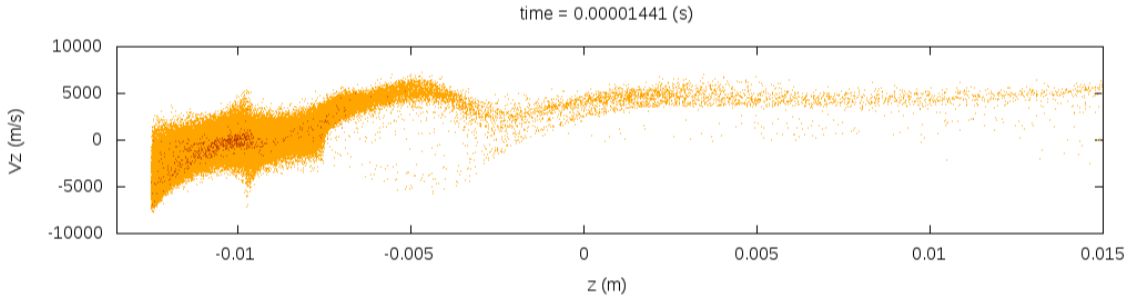

Figure 6.14. Particles velocity V_z with a 10^{20} plasma rate

6.2.2.1 Electric Potential

The electric potential for all simulations are presented bellow. According to the images the electron particles were moving as expected, since the plasma rate is now constant.

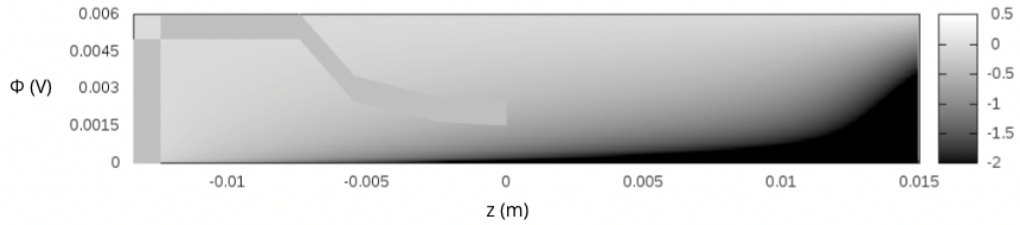

Figure 6.15. Electric potential of configuration 2 - 11 Radial

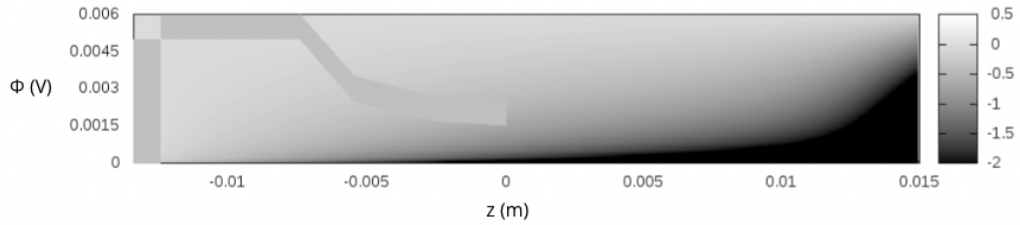

Figure 6.16. Electric potential of configuration 2 - 11 Axial

6.2.2.2 Particles position

The particles position has an specific condition for radial configurations, figures 6.20 6.22. The electrons are not displayed in the image, indeed one can see three points with high zoom

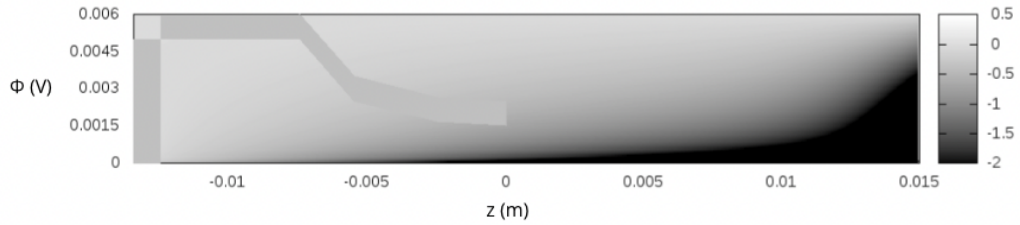

Figure 6.17. Electric potential of configuration 2 - 12 Radial

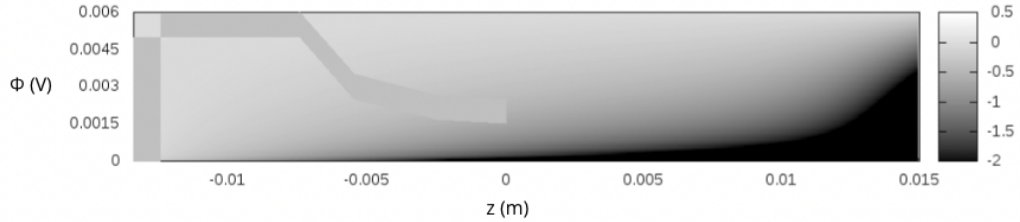

Figure 6.18. Electric potential of configuration 2 - 12 Axial

in. Despite it's disappearance, the position of ion particles remains the same throughout the experiment.

For the Axial representation, the behave is as expected. The particles insides the ionization chamber do follow the magnetic field line and the ion particles are able to follow them.

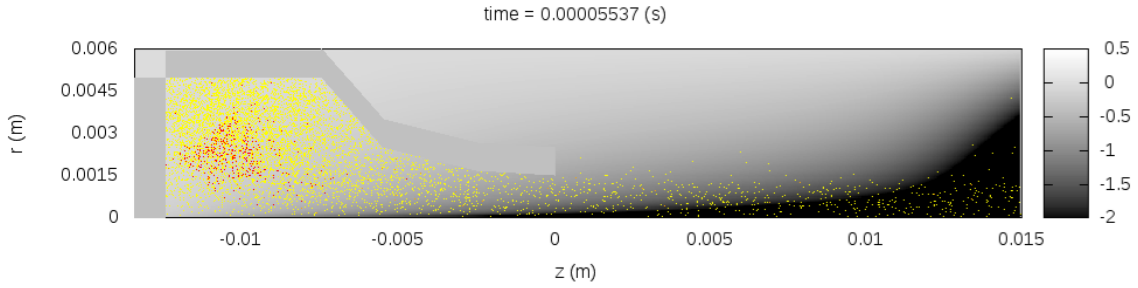

Figure 6.19. Ions and electrons positions of configuration 2 - 11 Axial, respectively yellow and red

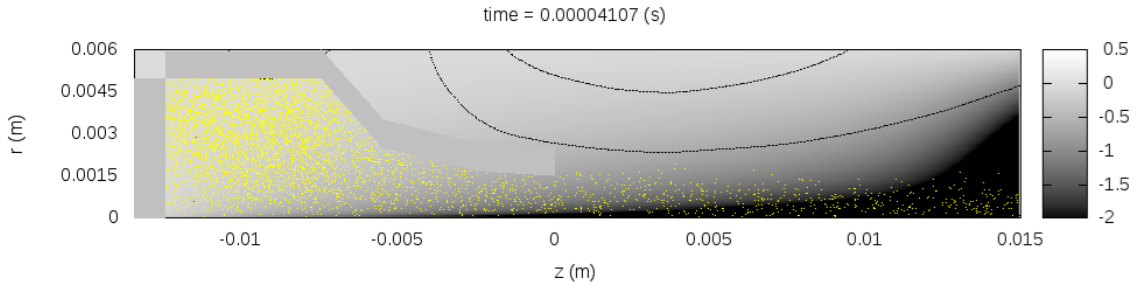

Figure 6.20. Ions and electrons positions of configuration 2 - 11 Radial, respectively yellow and red

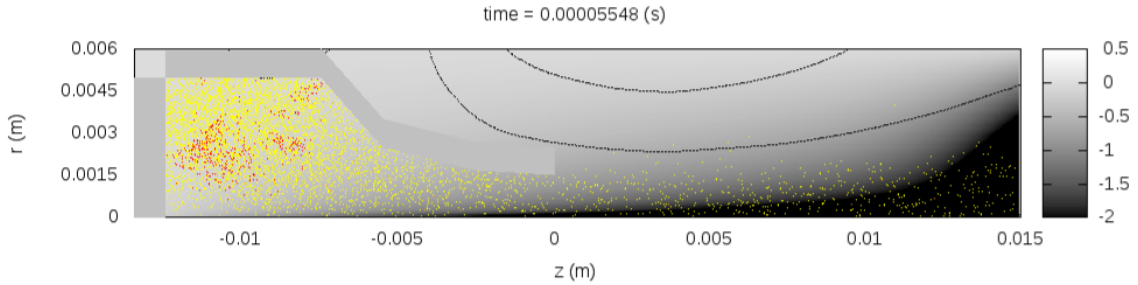

Figure 6.21. Ions and electrons positions of configuration 2 - 12 Axial, respectively yellow and red

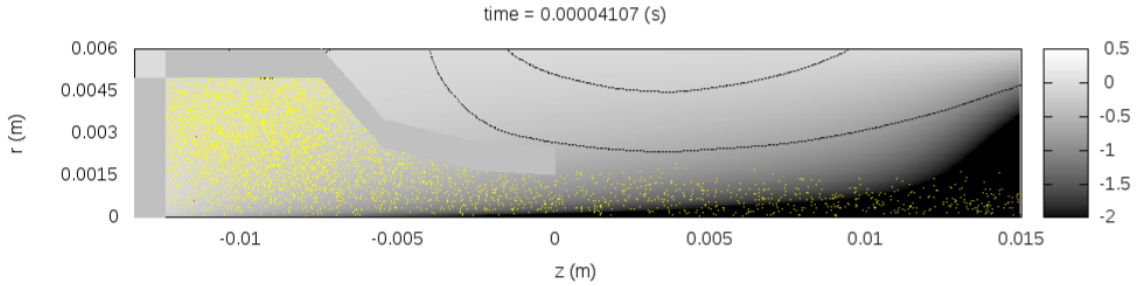

Figure 6.22. Ions and electrons positions of configuration 2 - 12 Radial, respectively yellow and red

6.2.2.3 Particles velocities

The last parameter is the particles velocities. The tabel 6.3 express the average velocities from the $z > 0.014$, as mentioned, in order to account the most efficient values of velocity.

The images represent the increase of velocity along the axis.The negative numbers concentrated in the ionization chamber zone, $z > -0.01$ and $z < 0$, represent the trapped ions. As the velocity does not increase considerably, it is considered that the particles are not reflecting back towards the plasma source. The positive inclination from $z > 0$ to $z < 0.015$ shows that the particles are moving positively into the exhaust direction. Even with a anomaly occuring, the Radial simulation presents a higher exhaust value.

This values ends the results and discussion and a conclusion is able to be taken to validate the research.

Table 6.3. Velocities for different magnet distance

Magnet configuration	V_z (m/s)
11mm radial	2.760e+03
12mm radial	2.760e+03
11mm axial	2.622e+03
12mm axial	2.359e+03

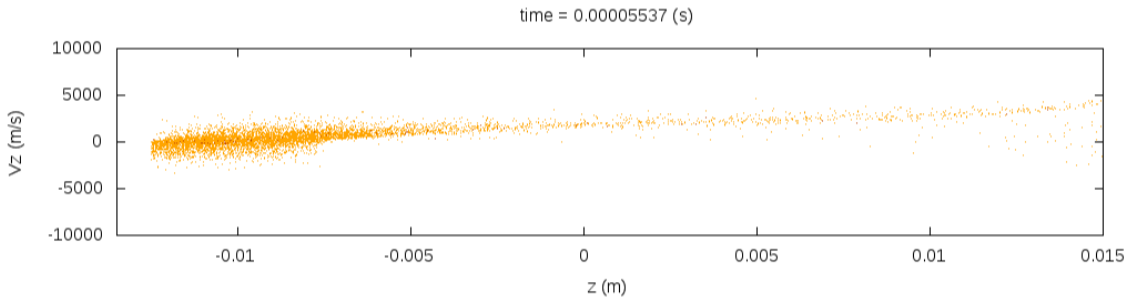

Figure 6.23. Velocit V_z of configuration 2 - 11 Axial

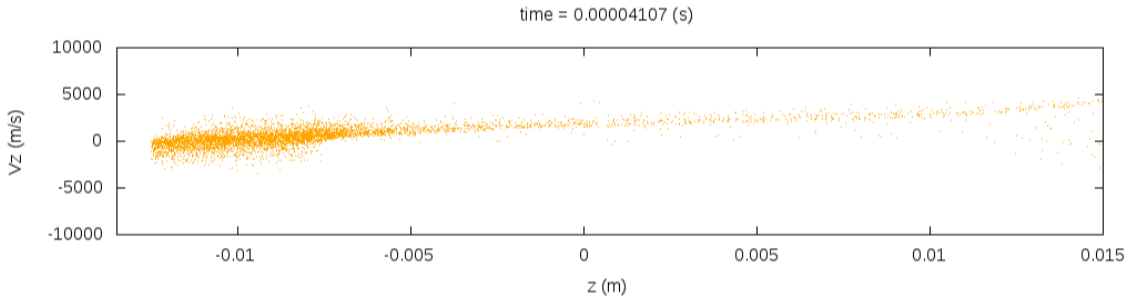

Figure 6.24. Velocit V_z of configuration 2 - 11 Radial

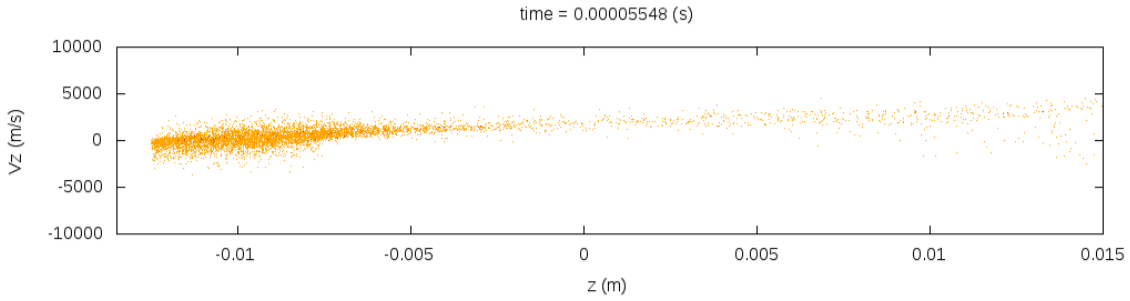

Figure 6.25. Velocit V_z of configuration 2 - 12 Axial

6.2.3 Specific impulse

The last parameter to be observed is the specific impulse generated from each system using the equation 3.4. The specific impulse is the last parameter able to define new constrains to the system and show efficiency from the design.

Beginning from the plasma rate, as velocities increases with plasma density, it is expected that the values of I_{sp} increase accordingly.

The magnet configuration had a different output and the radial set up also showed higher specific impulse values. As for the axial, the values are not as high. However the difference between the values is not high and this is a crucial asset for trade-off analysis.

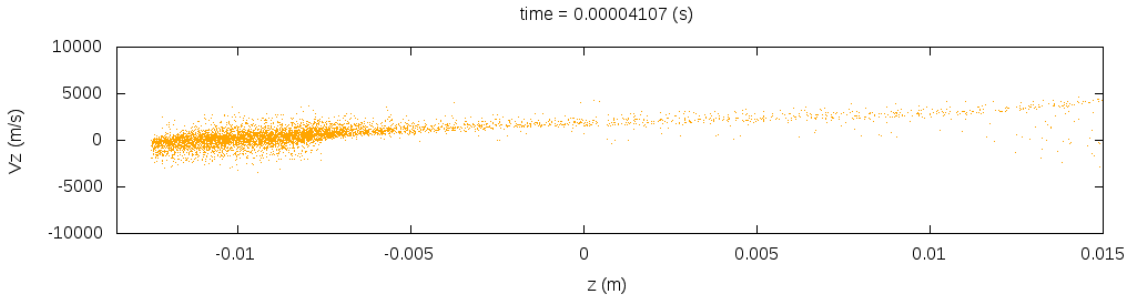

Figure 6.26. Velocit V_z of configuration 2 - 12 Radial

Table 6.4. Specific impulse for different plasma rate

Plasma rate	I_{sp} (s)
10^{16}	3.970800e+02
10^{18}	4.159060e+02
10^{20}	5.083540e+02

Table 6.5. Specific impulse for different magnet distance

Magnet configuration	I_{sp} (s)
11mm radial	3.843040e+02
12mm radial	3.843040e+02
11mm axial	3.620150e+02
12mm axial	3.624740e+02

7 Conclusion

The simulation and analyses conducted in this work demonstrate a balance required to optimize a plasma thruster design, in this case for PocketQube satellites. By evaluating magnetic field configurations, plasma source rates, and particles dynamics and specific impulse some insights emerge.

Table 7.1. Velocity and Specific impulse for different plasma rate

Magnet configuration	V_z (m/s)	I_{sp} (s)
10^{16}	2.3606e+03	3.970800e+02
10^{18}	3.3043e+03	4.159060e+02
10^{20}	4.37188e+03	5.083540e+02

Increasing the plasma source rate increased the exhaust velocities, as expected. Nevertheless, high rates generated instabilities in the system, for instance localized electric potential, unintended particle accumulation near the gas inlet and nozzle wall. These suggest that the high value are incompatible with the system design, as the density increases, they can compromise the system stability and even interfere with other subsystem inside the PQ.

Table 7.2. Velocity and Specific impulse for different magnet distance

Magnet configuration	V_z (m/s)	I_{sp} (s)
11mm axial	2.760e+03	3.843040e+02
12mm axial	2.760e+03	3.843040e+02
11mm radial	2.622e+03	3.620150e+02
12mm radial	2.359e+03	3.624740e+02

The radial magnetization proved effective in concentrating magnetic field lines within the ionization chamber, enhancing plasma confinement and potentially improving ionization efficiency. However this configuration showed limitations to achieve high exhaust velocities.

Axial magnetization in comparison had slightly weaker magnetic fields resulting in more efficient particle exhaust. The alignment of magnetic lines with the thruster longitudinal axis provided an efficient plasma flow toward the nozzle, reducing particle reflection or trapping. Thus this configuration had a better thrust efficiency.

The magnetic field lines simulations using FEMM also provided a precise evaluation of electron path, which where used to analyze plasma flow. As the ions are heavier they had a higher divergence of velocity distributions, due to dispersion following the magnetic lines. A further research to underline the magnetic design to minimize losses due to ions distribution is

required.

The simulations proposed in the work show an useful and efficient integration between FEMM and XOOPIC for plasma simulations. Some recommendations for further research also arise, such as:

- Optimization of radial magnetization configurations, in order to understand which distance is the most efficient;
- Analyze lower plasma rates and compare with experimental data from experiments run inside the LPF-UnB;
- Development of ionization process for PIC simulations to better understand power constrains and also gas ionization;
- Mission analysis for validation of best suitable mission for the EPS;
- Experimental validation and integration with power system to advance TRL level.

The values presented on tables 7.1 and 7.2, highlights values predicted in the literature, therefore proving the feasibility of miniaturizing the APT for PQ satellites.

Reference List

Ahedo, E. (2013). Plasma dynamics in a helicon thruster. Progress in Propulsion Physics, 4:337–354.

Alfriend, K., Vadali, S. R., Gurfil, P., How, J., and Breger, L. (2009). Spacecraft formation flying: Dynamics, control and navigation, volume 2. Elsevier.

Batishchev, O. V. (2009). Minihelicon plasma thruster. IEEE Transactions on plasma science, 37(8):1563–1571.

Bittencourt, J. A. (2013). Fundamentals of plasma physics. Springer Science & Business Media.

Bouwmeester, J., Gill, E., Speretta, S., and Uludag, S. (2017). A new approach on the physical architecture of cubesats & pocketqubes. In Proceedings of the 15th Reinventing Space Conference, Glasgow, UK, páginas 24–26.

Bouwmeester, J., Radu, S., Uludag, M., Chronas, N., Speretta, S., Menicucci, A., and Gill, E. (2020). Utility and constraints of pocketqubes. CEAS Space Journal, 12:573–586.

Charles, C. and Boswell, R. (2003). Current-free double-layer formation in a high-density helicon discharge. Applied Physics Letters, 82(9):1356–1358.

Chen, F. F. et al. (1984). Introduction to plasma physics and controlled fusion, volume 1. Springer.

Ebersohn, F. H., Sheehan, J., Longmier, B. W., and Shebalin, J. (2014). Quasi-one-dimensional code for particle-in-cell simulation of magnetic nozzle expansion. In 50th AIAA/ASME/SAE/ASEE Joint Propulsion Conference, página 4027.

Goebel, D. M., Katz, I., and Mikellides, I. G. (2023). Fundamentals of electric propulsion. John Wiley & Sons.

Hamrang, A. (2014). Advanced Non-Classical Materials with Complex Behavior: Modeling and Applications, volume 1. CRC Press.

Iannarelli, D., Ingenito, A., Napoli, F., Cichocki, F., Castaldo, C., De Ninno, A., Mannori, S., Cardinali, A., and Taccogna, F. (2024). Full helicon thruster modeling. arXiv preprint arXiv:2407.21457.

Jahn, R. G. (2006). Physics of electric propulsion. Courier Corporation.

Krejci, D. and Lozano, P. (2018). Space propulsion technology for small spacecraft. Proceedings of the IEEE, 106(3):362–378.

Kuwahara, D., Shinohara, S., Ishii, T., Otsuka, S., Nakagawa, T., Kishi, K., Sakata, M., Tanaka, E., Iwaya, H., Takizawa, K., et al. (2016). High-density helicon plasma thrusters using electrodeless acceleration schemes. Transactions of the Japan Society for Aeronautical and Space Sciences, Aerospace Technology Japan, 14(ists30):Pb_117–Pb_121.

Laufer, R. and Pelton, J. N. (2019). The smallest classes of small satellites including femtosats, picosats, nanosats, and cubesats. Handbook of Small Satellites: Technology, Design, Manufacture, Applications, Economics and Regulation, páginas 1–15.

Leomanni, M., Garulli, A., Giannitrapani, A., and Scortecci, F. (2017). Propulsion options for very low earth orbit microsatellites. Acta Astronautica, 133:444–454.

Levchenko, I., Xu, S., Mazouffre, S., Lev, D., Pedrini, D., Goebel, D., Garrigues, L., Taccogna, F., and Bazaka, K. (2020). Perspectives, frontiers, and new horizons for plasma-based space electric propulsion. Physics of Plasmas, 27(2).

Mejía-Kaiser, M. (2020). Iadc space debris mitigation guidelines. In The Geostationary Ring, páginas 381–389. Brill Nijhoff.

Merino, M. (2013). Analysis of magnetic nozzles for space plasma thrusters. PhD thesis, PhD Thesis, Polytechnic University of Madrid.

Miranda, R. A., Da Trindade, D. B., Luz, J. M. d. J., da Costa, S., and Ferreira, J. L. (2019). Particle-in-cell model of the helicon plasma thruster experiment at the university of brasilia. In Journal of Physics: Conference Series, volume 1365, página 012009. IOP Publishing.

Mueller, J., Hofer, R., and Ziemer, J. (2010). Survey of propulsion technologies applicable to cubesats. In Joint Army-Navy-NASA-Air Force (JANNAF), Colorado Springs, Colorado, May 3, 2010.

Musso, I., Manente, M., Carlsson, J., Giacomuzzo, C., Pavarin, D., Angrilli, F., and Bramanti, C. (2007). 2d oopic simulations of the helicon double layer. In 30th International Electric Propulsion Meeting, Florence, Italy-September, páginas 17–20.

NASA Small Spacecraft Systems Virtual Institute (2025). In-space propulsion. Accessed: February 16, 2025.

Navarro-Cavallé, J., Wijnen, M., Fajardo, P., Ahedo, E., Gómez, V., Giménez, A., and Ruiz, M. (2019). Development and characterization of the helicon plasma thruster prototype hpt05m. In Proceedings of the 36th International Electric Propulsion Conference.

Radu, S., Uludag, M., Speretta, S., Bouwmeester, J., Gill, E., and Foteinakis, N. (2018). Delfi-pq: The first pocketqube of delft university of technology. In 69th International Astronautical Congress, Bremen, Germany, IAC, páginas 1–10.

Sabale, A. and Adams, J. (2024). Systems engineering of a mars habitat using smad. In AIAA SCITECH 2024 Forum, página 1668.

Sammut, M., Azzopardi, M. A., and Fenech, M. (2019). Development of pulsed plasma thruster for a pocketqube pico-satellite.

Sheehan, J., Collard, T. A., Ebersohn, F. H., and Longmier, B. W. (2015). Initial operation of the cubesat ambipolar thruster.

Silva, M. A., Guerrieri, D. C., Cervone, A., and Gill, E. (2018). A review of mems micropropulsion technologies for cubesats and pocketqubes. Acta Astronautica, 143:234–243.

Smith, F. and Bae, J. (2023). Design, development, and testing of a low-cost sub-joule μppt for a pocket-cube. Aerospace, 10(3):316.

Squire, J. P., Díaz, F. C., Glover, T., Jacobson, V., Chavers, D., Bengtson, R., Bering III, E., Boswell, R., Goulding, R., and Light, M. (2003). Progress in experimental research of the vasimr engine. Fusion science and technology, 43(1T):111–117.

Tummala, A. R. and Dutta, A. (2017). An overview of cube-satellite propulsion technologies and trends. Aerospace, 4(4):58.

van Lynden, W. (2023). Mupets: A multi-regime plasma equilibrium transport solver for predicting ambipolar plasma thruster behaviour and performance.

Wachs, B. and Jorns, B. (2021). Optimization of an ecr thruster using two frequency and pulsed waveforms. In AIAA Propulsion and Energy 2021 Forum, página 3382.

Wasa, K. and Hayakawa, S. (1992). Handbook of sputter deposition technology.

Williams, L. T. and Walker, M. L. (2015). Plume structure and ion acceleration of a helicon plasma source. IEEE Transactions on Plasma Science, 43(5):1694–1705.

Yeo, S. H., Ogawa, H., Matthias, P., Kahnfeld, D., and Schneider, R. (2020). Multiobjective optimization and particle-in-cell simulation of cusped field thrusters for microsatellite platforms. Journal of Spacecraft and Rockets, 57(3):603–611.

York, T. M., Jacoby, B. A., and Mikellides, P. (1992). Plasma flow processes within magnetic nozzle configurations. Journal of propulsion and Power, 8(5):1023–1030.

Zanola, S. (2019). Assessment of the impact of miniaturized electric propulsion systems on small satellites technology. PhD thesis, Politecnico di Torino.